Letter

Enigmatic color centers in microdiamonds with bright, stable, and narrow-band fluorescence

Arthur Yu. Neliubov,[1,2,*] Ivan Yu. Eremchev,[2,3] Vladimir P. Drachev,[1] Sergey S. Kosolobov,[1] Evgeny A. Ekimov,[4] Artem I. Arzhanov,[2,3,5] Aleksandr O. Tarasevich,[5] and Andrey V. Naumov[2,3,5]

[1]*Skolkovo Institute of Science and Technology, Moscow 121205, Russia*
[2]*Moscow Pedagogical State University, Moscow 119435, Russia*
[3]*Institute for Spectroscopy of the Russian Academy of Sciences, Moscow, Troitsk 108840, Russia*
[4]*Institute for High Pressure Physics, Russian Academy of Sciences, Moscow, Troitsk 108840, Russia*
[5]*Lebedev Physical Institute of the Russian Academy of Sciences, Troitsk Branch, Moscow, Troitsk 108840, Russia*

(Received 28 September 2022; accepted 6 February 2023; published 28 February 2023)

Microdiamonds with color centers have unique photophysical properties. We discover extremely narrow spectral lines with full width at half maximum down to 0.5 nm (≈390 GHz at wavelength 630.15 nm) at room temperature in photoluminescence of numerous high-pressure–high-temperature microdiamonds. Correlation spectroscopy proves that these lines originate from single photon emitters. Comprehensive experimental characterization of the emitters is performed by means of complementary scanning electron and fluorescence microscopy that allows morphological characterization and in time monitoring of the same labeled emitters. Study of photoluminescence and photoluminescence excitation spectra of single emitters showed negligible phonon sideband and narrowband excitation. Temperature sensitivity, stable photoluminescence, brightness, linear polarization, and fluorescence lifetime ≈1.5–2.5 ns are demonstrated. The results show great potential of the discovered "enigmatic" emitters for applications in quantum optics, fluorescence labeling, and high-resolution thermometry.

DOI: 10.1103/PhysRevB.107.L081406

Diamonds with impurity centers, for instance, nitrogen vacancy (NV) [1,2], promise a broad range of applications such as quantum information [3–9], biomarking [10–13], all-optical sensors for highly sensitive magnetometry [8,14,10,15], and thermometry [16–18] at nanoscale. While NV is the most studied impurity center, there are some limitations for its applicability, such as a small Debye-Waller factor of 19% [relative intensity of zero-phonon lines (ZPLs)], lack of brightness, and transitions between charge states, that greatly alter the photoluminescence (PL) spectrum [19]. A list of impurity centers is expanded by introducing other elements of the periodic table to the diamond lattice and now includes more than a dozen types of defects [19,20]. Photoluminescence spectra of known color centers cover a broad range from blue to near infrared [21]. The most attractive impurities are group-IV elements, such as Si [22–27], Ge [28–33], and Sn [34–36], which form split-vacancy structure with D_{3d} symmetry class as opposed to C_{3v} class for NV centers [37]. It was reported that group-IV impurities possess better fluorescent properties such as higher photostability, narrower ZPL, and higher Debye-Waller factor [38]. ZPL spectral positions of SiV, GeV, and SnV centers are at 738, 602, and 619 nm, respectively. Importantly, these wavelengths correspond to biotransparency windows [21]. Common values of full width at half maximum (FWHM) for these color centers are about 5–7 nm at room temperature depending on the synthesis method [22,28,34]. The fluorescence lifetime takes values from 1 to 8 ns [39,40,31,34] for group-IV impurities and about 20 ns for NV^- centers [39]. Besides well-described color centers there are several emitters in diamond whose nature has not been identified yet. Recently reported new color centers, ST1 [41] and L1 [42], both were observed in ion implanted diamonds, while Si-related unidentified color centers were found in chemical vapor deposition (CVD)-made nanodiamonds [43]. ST1 color centers were later found in natural diamonds and are believed to be oxygen related impurity-vacancy centers [44]. As opposed to known color centers, ST1 shows optically detected magnetic resonance and allows for spin coherent control at room temperature [41]. The nature of L1 color centers is still unknown. L1 centers show a narrow (FWHM < 1.4 nm at room temperature), highly polarized line at wavelength 582 nm with weak vibronic sideband, and fluorescence lifetime about 2 ns [42].

Here we report the comprehensive study of another set of spectral lines in photoluminescence of high-pressure–high-temperature (HPHT) microdiamonds. These spectral lines are bright and narrow band with minimal FWHM of 0.52 nm. Observed lines do not correspond to the spectra of any known defects in diamond [20], but appear to possess similar properties to L1 centers in terms of polarization degree and lifetime. The lines are found in multiple microcrystals from different samples. We relate lines to photoluminescence of yet unidentified impurity centers. Further, we will call them LX as they have similar features like L1 in Ref. [42]. Importantly, the observed LX centers show better fluorescence

*arthur.neliubov@skoltech.ru

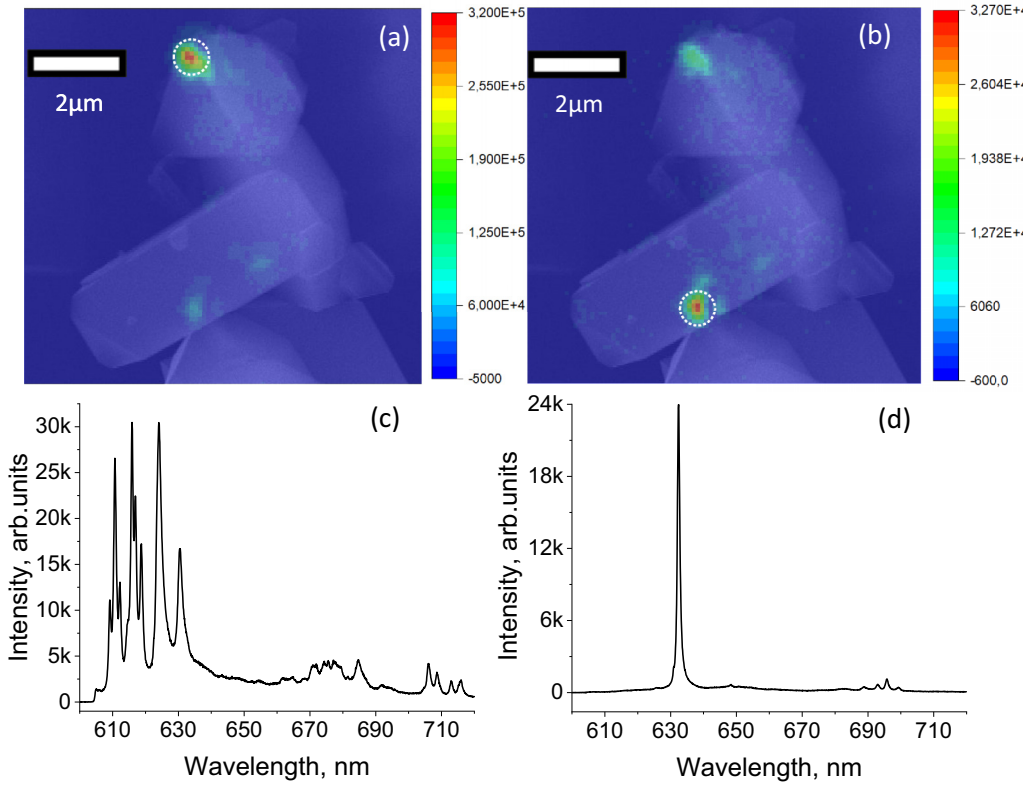

FIG. 1. (a), (b) Combination of SEM image and photoluminescence intensity map (semitransparent), excitation wavelength 590.5 nm. Integral photoluminescence over spectral region (a) 605–640 nm and (b) 629–633 nm was collected while constructing the photoluminescence map, showing positions of two separated light sources. (c) PL spectrum of upper emitter in panel (a) with several lines and (d) PL spectrum of bottom emitter in panel (b) with single line.

properties, comparing to the known color centers, and have great potential for various applications. The aim of this Letter is to give precise and comprehensive characterization of discovered color centers to shed light on their nature and thereby allow on demand synthesis of such color centers. To do that we developed a method for complementary scanning electron microscopy (SEM) and spectroscopic fluorescent microscopy by labeling diamonds of highest interest on a matrix with arrays of cells. This method allows performing a series of different experiments with the same objects.

For this purpose, we designed special substrates fabricated with electron-beam lithography, suitable for both microscopes. Our approach allows us to label diamonds of highest interest. A confocal fluorescent microscope with access to a spectrometer and the Hanbury Brown and Twiss scheme were used for optical properties studies. Tunable continuous wave and pulsed lasers were used as excitation source. Visualization of the diamonds and elemental analysis were performed with scanning electron microscopes. See Supplemental Material for details of experimental techniques [45]. Three consignments of HPHT microdiamonds were analyzed in this Letter. Initially we observed unidentified lines in Ge-doped microdiamonds. Then we concentrated on two consignments of diamonds without intentional impurity implementation, "pure" diamonds. For details of the synthesis see Supplemental Material [45] and Ref. [46] therein.

Multiple unidentified narrow and intensive spectral lines were observed in PL spectra of HPHT microdiamonds at room temperature. Unknown lines appeared in numerous microdiamonds. They are present in both clusterlike diamonds and single monocrystals. One of them is shown in Fig. 1 with PL maps in spectral ranges 605–640 nm [Fig. 1(a)] and 629–633 nm [Fig. 1(b)], and excitation wavelength 590.5 nm. One can see several narrow overlapping lines [Fig. 1(c)] in the diffraction limited area corresponding to the upper bright spot in Fig. 1(a). We see a single line spectrum [Fig. 1(d)] collected from the bright spot shown at the bottom of Fig. 1(b). It is not clear though whether these spectra originate from emission of several emitters or just one. To clarify that, we measure the second-order correlation function for particular lines, where it is possible. In most cases, allocated single spectral lines demonstrate deep antibunching and therefore originate from single color centers. However, the integral signals from several lines correspond only to partial antibunching at best, which evidences ensemble structure.

Note, that the lines are observed in dozens of different crystals on different substrates with different sample application techniques. The substrates were cleaned thoroughly during sample preparation. We investigated 20 crystals with 85 unidentified intensive lines to collect statistics. The lines are spread out over a spectral range of 600–650 nm as illustrated in Fig. 2(a). That is not common for the color centers known in

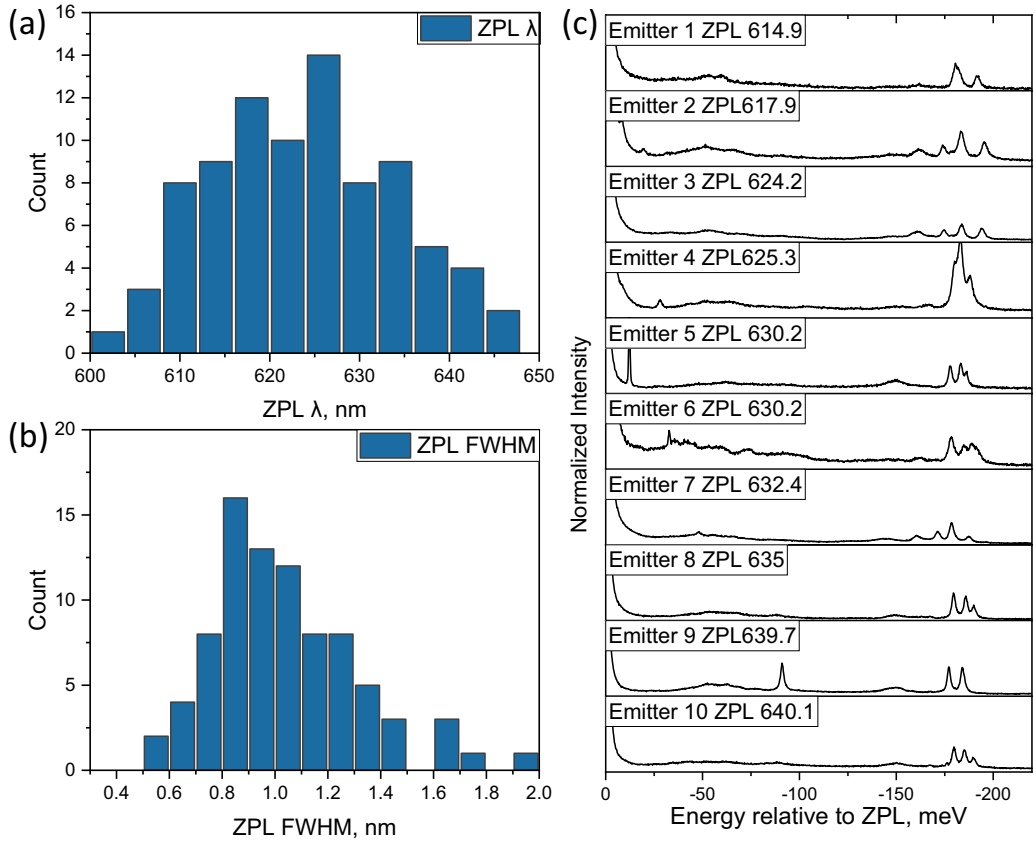

FIG. 2. Statistics of observed spectral lines. (a), (b) Distribution of ZPL position and FWHM respectively. (c) PL spectra of phonon sideband of ten emitters. The x axis is constructed in energy units while ZPL energy is subtracted, intensity is normalized to the maximum of the line, and scale is the same for all emitters.

the literature. Although ZPL positions of GeV, PbV, and NV^- color centers are 602, 619, and 637 nm, correspondently, the variation of their spectral position is an order of magnitude less than the spectral range of our centers and present in case of extreme lattice stresses. It should be noted that no spectral diffusion was observed in our experiments (see Supplemental Material [45] for more information). The characteristic linewidths of well-known group-IV defects in diamonds are about 5 nm for high quality diamonds [22,28,34]. In our lines the average FWHM is about 800 GHz (1.1 nm) with minimal value 390 GHz (0.52 nm) [see histogram in Fig. 2(b)]. In the case of multiple lines, the spectra of different emitters overlap and therefore it is difficult to analyze spectral structure [Fig. 1(c)]. Hence, we are focused on analyzing objects with a single ZPL like in Fig. 1(d). To compare spectral structure of LX centers, scales are built in energy units with subtracted value of ZPL energy for each emitter [Fig. 2(c)]. Clearly, spectral structures for different single emitters are similar, even though the spectral position of ZPL varies significantly. As it is shown in Fig. 2(c) the spectra consist of a ZPL, a wide small phonon sideband (PSB) with maximum at ≈50 meV (PSB), and three pronounced narrow vibronic replicas at ≈170–200 meV. These features are not common for vibration spectra of pure diamonds [20] and appear due to the presence of defect centers. The pronounced phonon sideband, while typical for the known color centers, is almost negligible in our case of LX centers. Note again, the L1 centers [42] have also quite small PSB. In addition to the fact that the ZPL energies for the different color centers vary, the structure of the vibronic replicas is also not exactly the same. The relative shifts and intensities of these features varied for different LX centers, once again indicating the difference of local conditions.

Discovered color centers demonstrate similar spectra and properties, even though the position of ZPL is distributed over a broad range. Recent study of GeV-center photoluminescence in CVD bulk diamonds showed inhomogeneous broadening of ZPL which correlates with morphological inhomogeneity (see Ref. [47] and references therein). Similarly, the discovered spectral lines could correspond to color centers of the same type but in significantly different local conditions, which cause a variation of ZPL positions.

In order to characterize observed LX centers, we performed a series of different experiments with the same single LX center, emitter N8 from Fig. 2(c), which was the only emitter found in a single microdiamond, shown in Fig. 3(d). The intensity correlation function shows well-resolved antibunching behavior in continuous and pulsed excitation regimes with values $g^2(0) = 0.2$ and 0.04, respectively [Fig. 3(a)]. This proves that the line is originated from a single emitter. The measured lifetime of PL is about 1.9 ns, which is close to the values for SiV and GeV [40,31] centers. For other LX centers lifetime varied in the range 1.5–2.5 ns. Stable photoluminescence is observed up to excitation

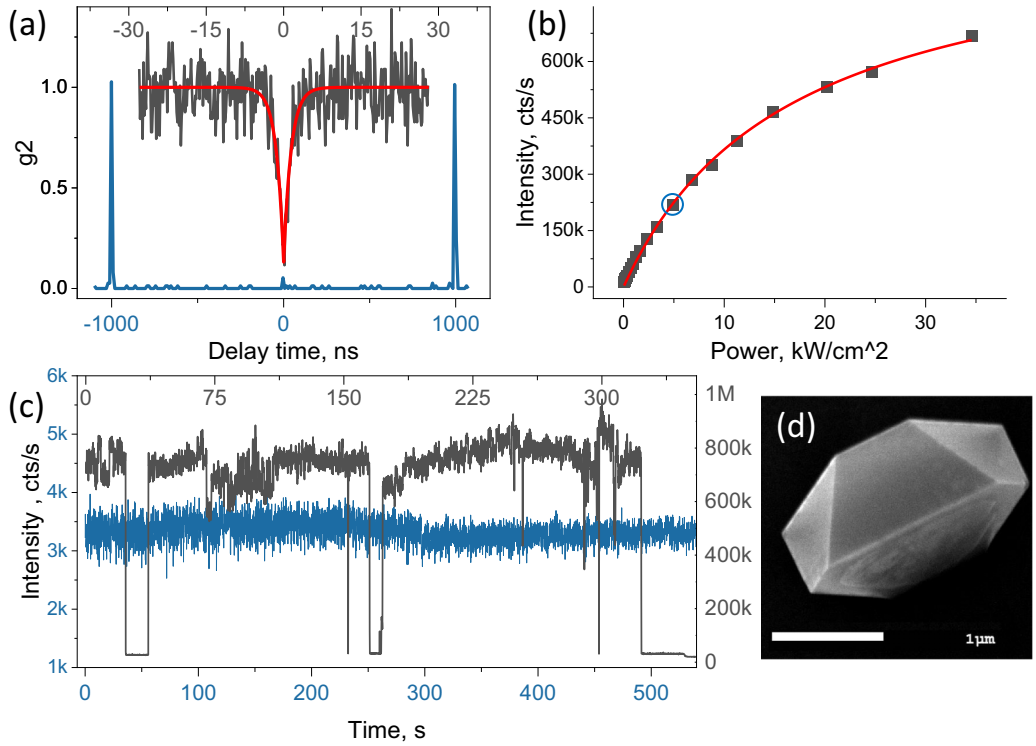

FIG. 3. Photoluminescence properties of a single LX-color center. (a) Second-order autocorrelation functions for continuous and pulsed excitation giving values of $g^2(0) = 0.2$ and 0.04 respectively, which proves that ZPL 635 nm corresponds to a single emitter. (b) Saturation dependence with estimated $P_{sat} = 15.5\,\mathrm{kW/cm^2}$ and $I_\infty = 9.3 \times 10^5$. Blue circle indicates the point when blinking begins. (c) Fluorescent track of emitter showing stable fluorescence over 8-min range at low excitation power density 1.7 kW/cm^2 (blue) and pronounced blinking at high power 450 kW/cm^2 with photodegradation after 500 s exposure (gray). (d) SEM image of a crystal with emitter N8.

power density 4.9 kW/cm^2 [Fig. 3(c) blue]. A following power increase is accompanied by blinking. Longer off states are observed at an intensity of about 450 kW/cm^2 [Fig. 3(c) gray]. Exposure of the color center for 500 s at this power led to irreversible photodegradation of the considered emitter.

Power dependent saturation measurements were fitted with the saturation law, defined by Eq. (1):

$$I = I_\infty \frac{P}{P + P_{sat}} \tag{1}$$

where I_∞ stands for saturation intensity, and P_{sat} stands for saturation power density [Fig. 3(b)]. Saturation count rate and power density obtained from fitting are $I_\infty = 9.310^5$ counts/s and $P_{sat} = 15.5$ kW/cm^2. The calculated value of the maximum count rate of the collected fluorescence, assuming that each cycle of excitation-relaxation results in one emitted photon, is defined by Eq. (2):

$$I_{max} = \frac{k}{\tau} = 5.2 \times 10^7 \text{ counts/s} \tag{2}$$

where $k \approx 0.1$ is experimental setup collection efficiency for the isotropically emitting point source [45], and $\tau = 1.9$ ns is the fluorescence lifetime. We assume that difference in experimental and calculated saturation count rates could be the result of limited quantum yield of photoluminescence due to presence of nonradiative relaxation channels. Existence of a metastable level with relatively high lifetime could also limit experimental count rate. Besides, collection efficiency is probably overestimated, because our calculation does not account for the direction of the emitter's dipole moment in relation to the surfaces of microdiamond. Indeed, because of large contrast in refractive indices of air ($n = 1$) and diamond ($n = 2.4$) the angle of total internal reflection is only 24.6° for photoluminescence of color centers, which can limit the photon flux in the detection direction. Designing special nanostructures or covering diamonds with solid immersion lenses can help to improve the collection efficiency and/or enhance spontaneous emission [19].

As we mentioned above, the PL spectra of different LX centers have similar structures of the spectrum, which consist of narrow ZPLs, insignificant PSB, and vibronic replicas. The detailed PL spectrum of emitter N8 is shown below in Fig. 4(a). The PL spectrum at excitation at wavelength 580.5 nm is shown in black. It consists of narrow (FWHM = 0.58 nm) and intensive ZPL at wavelength 635 nm, weak phonon sideband (Debye Waller factor ≈ 70%), and vibronic replicas. Detailed vibration spectra under excitation at wavelength 634.7 nm (wavelength of ZPL) recorded with higher exposure time are shown in blue in Fig. 4(a). Black and blue graphs coincide with high accuracy if normalized, which verifies that all the signals originate from the same single LX center and the level of background signal is negligible. We see three intensive narrow features with energies 180, 186.4, and 190.6 meV, which are the first vibronic replicas. Signal with higher (>200 meV) energy shift appears to repeat the structure of the phonon sideband. Four distinct peaks with energies 359.4, 365.97, 370.5, and 376 meV [Fig. 4(a)] are likely to be the second vibronic replicas.

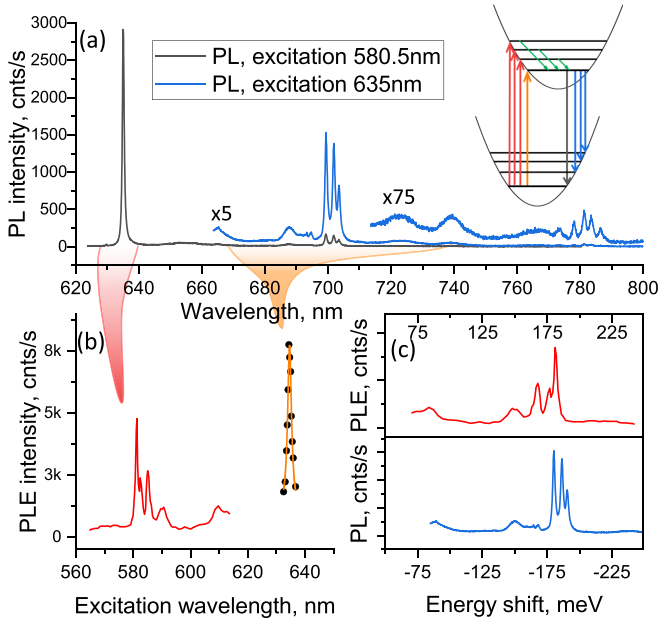

FIG. 4. Spectral properties of the investigated emitter at room temperature. (a) PL spectra of emitter N8 under excitation at wavelength 580.5 nm (black) and 635 nm (blue). Arrows show the wavelength of excitation. Blue graphs are multiplied by 5 and 75 to show the structure of the phonon sideband. Inset: Preliminary structure of energy levels. (b) PLE spectra of emitter N8. While constructing the left part of the spectra we analyzed integral intensity of the line 635 nm in photoluminescence (red) and while constructing the PLE spectrum of the ZPL we analyzed integral intensity of phonon sideband photoluminescence 670–740 nm (orange). Dashed line corresponds to the peak wavelength of photoluminescence ZPL. (c) Combined PLE (upper panel) and PL (lower panel) spectra of PSB. X scale is built in energy units with subtracted value of ZPL transition 1.954 eV for PLE and 1.953 eV for PL.

The photoluminescence excitation spectra (PLE) spectrum of LX centers is also of great interest. For emitter N8 the PLE spectrum [Fig. 4(b)] was measured in two modes.

(1) The laser was scanned in spectral range 564.5–612.7, while integral intensity of ZPL photoluminescence was analyzed. That mode helped us to study efficiency of nonresonant excitation of the emitter.

(2) The laser was scanned in the range of ZPL 632.5–637 nm and an integral signal of photoluminescence in range 670–730 was considered. That mode allowed us to understand the profile of ZPL in excitation and to calculate ZPL Stokes shift, which is measured to be 0.6 nm.

Clearly, the excitation spectrum is narrow band, which is one of the important peculiarities of LX centers. In Fig. 4(c) we show comparison of PLE and PL spectra of emitter N8 in energy units, and the energy of 0-0 transition (1.953-eV PL, 1.954-eV PLE) is subtracted. The structures of PL and PLE spectra look alike, but the position and intensity of the peaks, associated with vibronic replicas, are slightly different in cases of PL and PLE spectra. Such small deviation from mirror symmetry of PL and PLE spectra can be explained by joint influence of Franc-Condon and Herzberg-Teller interaction [48]. The most intensive peaks in excitation correspond to energies 167.7, 176.6, and 181.3 meV, while

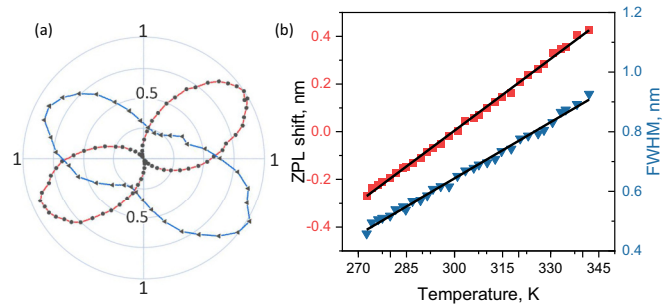

FIG. 5. (a) Radiation pattern of ZPL photoluminescence. Blue curve corresponds to PL polarization, while red represents PLE modulation. (b) Temperature-dependent measurements of position (red) and linewidth (blue) of ZPL.

in photoluminescence the most intensive peaks are 180, 186.4, and 190.6 meV. Similar excitation spectra are observed for other single LX centers. The characteristic value of the vibronic states' energy for LX centers is in the range 160–200 meV, while ZPL transition energy is in the range 1.9–2.06 eV. Thus, we see that effective excitation of LX centers is achieved not only for 0-0 transition, but also for transitions from the ground state to the discrete vibronic states. Narrow linewidth of vibronic replicas allows selective excitation of individual LX centers with large spectral shift between selective narrow-band excitation and ZPL photoluminescence by tuning laser wavelength, and that could be useful for real multicolor diagnostics [49] at room temperature.

A simplified energy level system with first discrete vibronic states is shown in the inset of Fig. 4(a). Red and blue arrows correspond to vibronic replicas features in excitation and photoluminescence, respectively. Green arrows demonstrate nonradiative relaxation.

Polarization patterns [Fig. 5(a)] are measured for two electron-vibrational energy transitions: in PL and in PLE. PL polarization dependence is measured for ZPL at 635 nm, indicated in blue in Fig. 5(a). PLE polarization dependence is measured for transition from the ground state to the vibronic level of the first excited state, shown in red in Fig. 5(a). For that we rotate the polarization of laser excitation at 580.8 nm, while analyzing intensity of ZPL in PL. The polarization contrast is given by Eq. (3):

$$C = \frac{I_{\max} - I_{\min}}{I_{\max} + I_{\min}}, \tag{3}$$

where $I_{\max}$ and $I_{\min}$ are maximum and minimum PL intensities at orthogonal polarizations. For the photoluminescence of the line 635 nm contrast was only 53%. The contrast of excitation was 98% which corresponds to a dipole transition polarization. Phase shift between the radiation patterns of emission and excitation could be explained by difference of dipole moment directions for 0-0 transition (PL) and for transition from the ground state to a vibronic replica state (PLE). It should be noted that for some other single emitters we observed almost 100% contrast of 0-0 transition in photoluminescence.

The other peculiarity of LX centers is great temperature sensitivity. For applications in all-optical thermometry researchers are interested in emitters with bright, temperature sensitive ZPL, that is an attribute of discovered emitters.

The dependencies of ZPL's linewidth and peak position on temperature are shown in Fig. 5(b). The ZPL linewidth changes approximately two times and peak position shows $\approx$ 0.7-nm shift in temperature interval 272–342 K. As we can see the linewidth and position of ZPL could be fitted with linear temperature dependency, which is explained with first-order electron-phonon interactions [25]. It worth noting that phototransformation of emitter N8 took place before temperature-dependent measurements, which resulted in slight shift of the ZPL from 635 to 633.9 nm. Therefore, the position of ZPL may not be the best parameter for measurement of absolute temperature, due to possible spectral diffusion. That is why FWHM is a more reliable parameter in temperature analysis. LX centers possess narrow and bright ZPL and weak PSB, and that is why accuracy of ZPL fitting could be better than for known color centers. Accuracy of temperature estimation at 100-ms exposure time achieved from LX-center linewidths measurements is 0.54 K near room temperature obtained from Eq. (4):

$$\sigma = \frac{\gamma}{s_\gamma * \sqrt{I}}, \tag{4}$$

where γ denotes linewidth, $s_\gamma = 0.0065\,\mathrm{nm/K}$ denotes temperature susceptibility of the linewidth, I denotes count rate $\approx 2.9 \times 10^5$ counts/s [excitation power density ≈ 7 kW/cm^2, which is near the blinking point; see Fig. 3(b)]. Even though the s_γ parameter is an order of magnitude smaller than in the case of SiV centers [50], high accuracy is achieved due to smaller linewidth and high count rate. Tracking a pair of ZPL parameters such as peak position and linewidth could give sufficient information about absolute value of temperature and its derivative, because tracking the peak of ZPL could result in even better accuracy. Also, it should be noted that the absolute temperature measurement requires calibration of each emitter. Nevertheless, this is a great result for further applications in bio- and medical nanothermometry.

To clarify the nature of observed LX centers we carried out annealing of some part of the diamonds in oxygen atmosphere at 600°C. Thus, we burned the possible contamination elements on the surface, so they could not contribute to emission. However, the lines, which correspond to LX centers, were still observable (see Supplemental Material [45]). Thus, we suppose that discovered spectral lines corresponded to defects inside microdiamonds.

Elemental analysis was performed using energy dispersive spectroscopy and time-of-flight–secondary ions mass spectroscopy (TOF-SIMS) for microdiamonds with relatively high concentration of LX centers. Neither method showed any unusual elements, that could have been contaminants during synthesis. The best resolution was achieved with TOF-SIMS method, $<$10 ppm. The list of detected elements consisted of carbon, silicon, oxygen, and nitrogen. Nitrogen was found in microdiamonds, even though NV-center emission was observed only in one crystal out of several dozen, which emphasizes the sensitivity of the method. L1 centers, which seem to be of similar nature, were found in CVD diamond after implantation with CN ions [43]. Hence, we suppose, that the observed spectral lines most likely originated from common contaminants of diamond such as nitrogen or silicon, that formed an unusual defect structure.

To conclude, we report narrow spectral lines with FWHM down to 0.52 nm at room temperature. These unidentified spectral lines in photoluminescence with narrow excitation spectra are emitted by "enigmatic" color centers in HPHT microdiamonds. For characterization of observed emitters, we developed a method of coordinated scanning electron microscopy and fluorescent spectroscopic microscopy, which allows monitoring of the objects, including single photon sources. Observed emitters are similar to L1 centers found in ion implanted CVD diamonds [42], but the ZPL appear in different spectral range (600–650 nm as opposed to 577–605 nm). We prove that single ZPLs are originated from single color centers. PL spectra of different single emitters have typical structure, namely, narrow and intensive ZPL, weak phonon sideband, and several vibronic features well resolved at room temperature. PLE spectra have also narrow-band structure, unlike other known color centers. PL and PLE spectra show small Stokes shift of ZPL of about 0.6 nm and little asymmetry. The value of fluorescence lifetime is about 1.5–2.5 ns, and the Debye-Waller factor is about 70%. Our color centers possess high brightness (single photon detection count rate 2.2×10^5 counts/s with saturation rate 9.3×10^5 counts/s). They have high photostability without blinking or bleaching at the laser excitation power density up to 4.9 kW/cm^2 and detected count rate of about 2.2×10^5 counts/s. The effect of PL blinking was observed with higher excitation power densities with characteristic on/off times by order of seconds during hundreds of seconds. Most of the luminescence signal is concentrated in narrow ZPL with pronounced polarization, which together with the spectral stability and single photon emission makes LX centers attractive single photon sources for quantum optics [51,52] and quantum cryptography [53]. Elemental analysis shows no signs of any atoms other than C, Si, O, and N in microcrystals with relatively high concentration of the discovered color centers. Narrow linewidth at room temperature, stable photoluminescence, and short lifetime demonstrate that discovered emitters are attractive for further development and engineering. Narrow effective excitation spectra open the ability to address discovered color centers individually, which is of high interest for real multicolor super-resolution diagnostics. High temperature sensitivity and lack of hysteresis make LX centers promising for applications in high resolution localization thermometry, with accuracy of $dT \approx 0.5$ K and detection exposure time of $\approx$100 ms for a single color center and moderate power density. This is a promising result for further applications in bio- and medical nanothermometry.

The data that support the findings of this Letter are available from the corresponding author upon reasonable request.

The authors acknowledge support by Lebedev Physical Institute of the Russian Academy of Sciences Task No. AAAA-A19-119083090053-9, Moscow Pedagogical State University Task No. AAAA-A20-120061890084-9, and Institute for Spectroscopy of the Russian Academy of Sciences Task No. FFUU-2022-0003. A.Y.N., I.Y.E., A.I.A., A.O.T.,

and A.V.N. are members of the Leading Scientific School of the Russian Federation (NSh-776.2022.1.2). The Advanced Imaging Core Facilities of Skoltech is acknowledged for granting access to SEM facilities.

[1] F. Jelezko and J. Wrachtrup, Single defect centres in diamond: A review, Phys. Status Solidi **203**, 3207 (2006).
[2] M. W. Doherty, N. B. Manson, P. Delaney, F. Jelezko, J. Wrachtrup, and L. C. Hollenberg, The nitrogen-vacancy colour centre in diamond, Phys. Rep. **528**, 1 (2013).
[3] J. Wrachtrup and F. Jelezko, Processing quantum information in diamond, J. Phys.: Condens. Matter **18**, S807 (2006).
[4] D. D. Awschalom, R. Hanson, J. Wrachtrup, and B. B. Zhou, Quantum technologies with optically interfaced solid-state spins, Nat. Photonics **12**, 516 (2018).
[5] G. Balasubramanian, P. Neumann, D. Twitchen, M. Markham, R. Kolesov, N. Mizuochi, J. Isoya, J. Achard, J. Beck, and J. Tissler, Ultralong spin coherence time in isotopically engineered diamond, Nat. Mater. **8**, 383 (2009).
[6] B. Grotz, M. V. Hauf, M. Dankerl, B. Naydenov, S. Pezzagna, J. Meijer, F. Jelezko, J. Wrachtrup, M. Stutzmann, and F. Reinhard, Charge state manipulation of qubits in diamond, Nat. Commun. **3**, 1 (2012).
[7] A. Gali, Theory of the neutral nitrogen-vacancy center in diamond and its application to the realization of a qubit, Phys. Rev. B **79**, 235210 (2009).
[8] S. Hong, M. S. Grinolds, L. M. Pham, D. Le Sage, L. Luan, R. L. Walsworth, and A. Yacoby, Nanoscale magnetometry with NV centers in diamond, MRS Bull. **38**, 155 (2013).
[9] S. Pezzagna and J. Meijer, Quantum computer based on color centers in diamond, Appl. Phys. Rev. **8**, 011308 (2021).
[10] D. R. Glenn, K. Lee, H. Park, R. Weissleder, A. Yacoby, M. D. Lukin, H. Lee, R. L. Walsworth, and C. B. Connolly, Single-cell magnetic imaging using a quantum diamond microscope, Nat. Methods **12**, 736 (2015).
[11] F. Morales-Zavala, N. Casanova-Morales, R. B. Gonzalez, A. Chandía-Cristi, L. D. Estrada, I. Alvizú, V. Waselowski, F. Guzman, S. Guerrero, and M. Oyarzún-Olave, Functionalization of stable fluorescent nanodiamonds towards reliable detection of biomarkers for Alzheimer's disease, J. Nanobiotechnol. **16**, 1 (2018).
[12] L. P. McGuinness, Y. Yan, A. Stacey, D. A. Simpson, L. T. Hall, D. Maclaurin, S. Prawer, P. Mulvaney, J. Wrachtrup, and F. Caruso, Quantum measurement and orientation tracking of fluorescent nanodiamonds inside living cells, Nat. Nanotechnol. **6**, 358 (2011).
[13] A. Mzyk, Y. Ong, A. R. Ortiz Moreno, S. K. Padamati, Y. Zhang, C. A. Reyes-San-Martin, and R. Schirhagl, Diamond color centers in diamonds for chemical and biochemical analysis and visualization, Anal. Chem. **94**, 225 (2022).
[14] L. Rondin, J.-P. Tetienne, T. Hingant, J.-F. Roch, P. Maletinsky, and V. Jacques, Magnetometry with nitrogen-vacancy defects in diamond, Rep. Prog. Phys. **77**, 056503 (2014).
[15] G. Balasubramanian, I. Chan, R. Kolesov, M. Al-Hmoud, J. Tisler, C. Shin, C. Kim, A. Wojcik, P. R. Hemmer, and A. Krueger, Nanoscale imaging magnetometry with diamond spins under ambient conditions, Nature (London) **455**, 648 (2008).
[16] T. Plakhotnik, M. W. Doherty, J. H. Cole, R. Chapman, and N. B. Manson, All-optical thermometry and thermal properties of the optically detected spin resonances of the NV-center in nanodiamond, Nano Lett. **14**, 4989 (2014).
[17] S. Sotoma, C. Zhong, J. C. Y. Kah, H. Yamashita, T. Plakhotnik, Y. Harada, and M. Suzuki, In situ measurements of intracellular thermal conductivity using heater-thermometer hybrid diamond nanosensors, Sci. Adv. **7**, eabd7888 (2021).
[18] A. M. Romshin, V. Zeeb, A. K. Martyanov, O. S. Kudryavtsev, D. G. Pasternak, V. S. Sedov, V. G. Ralchenko, A. G. Sinogeykin, and I. I. Vlasov, A new approach to precise mapping of local temperature fields in submicrometer aqueous volumes, Sci. Rep. **11**, 14228 (2021).
[19] K. Liu, S. Zhang, V. Ralchenko, P. Qiao, J. Zhao, G. Shu, L. Yang, J. Han, B. Dai, and J. Zhu, Tailoring of typical color centers in diamond for photonics, Adv. Mater. **33**, 2000891 (2021).
[20] A. M. Zaitsev, Vibronic spectra of impurity-related optical centers in diamond, Phys. Rev. B **61**, 12909 (2000).
[21] M. H. Alkahtani, F. Alghannam, L. Jiang, A. Almethen, A. A. Rampersaud, R. Brick, C. L. Gomes, M. O. Scully, and P. R. Hemmer, Fluorescent nanodiamonds: Past, present, and future, Nanophotonics **7**, 1423 (2018).
[22] W. Liu, M. N. A. Alam, Y. Liu, V. N. Agafonov, H. Qi, K. Koynov, V. A. Davydov, R. Uzbekov, U. Kaiser, and T. Lasser, Silicon-vacancy nanodiamonds as high performance near-infrared emitters for live-cell dual-color imaging and thermometry, Nano Lett. **22**, 2881 (2022).
[23] N. Morioka, C. Babin, R. Nagy, I. Gediz, E. Hesselmeier, D. Liu, M. Joliffe, M. Niethammer, D. Dasari, and V. Vorobyov, Spin-controlled generation of indistinguishable and distinguishable photons from silicon vacancy centres in silicon carbide, Nat. Commun. **11**, 1 (2020).
[24] R. Waltrich, B. Lubotzky, H. Abudayyeh, E. S. Steiger, K. G. Fehler, N. Lettner, V. A. Davydov, V. N. Agafonov, R. Rapaport, and A. Kubanek, High-purity single photons obtained with moderate-NA optics from SiV center in nanodiamonds on a bullseye antenna, New J. Phys. **23**, 113022 (2021).
[25] K. D. Jahnke, A. Sipahigil, J. M. Binder, M. W. Doherty, M. Metsch, L. J. Rogers, N. B. Manson, M. D. Lukin, and F. Jelezko, Electron-phonon processes of the silicon-vacancy centre in diamond, New J. Phys. **17**, 043011 (2015).
[26] L. J. Rogers, K. D. Jahnke, M. H. Metsch, A. Sipahigil, J. M. Binder, T. Teraji, H. Sumiya, J. Isoya, M. D. Lukin, and P. Hemmer, All-Optical Initialization, Readout, and Coherent Preparation of Single Silicon-Vacancy Spins in Diamond, Phys. Rev. Lett. **113**, 263602 (2014).
[27] L. J. Rogers, K. D. Jahnke, M. W. Doherty, A. Dietrich, L. P. McGuinness, C. Müller, T. Teraji, H. Sumiya, J. Isoya, and N. B. Manson, Electronic structure of the negatively charged silicon-vacancy center in diamond, Phys. Rev. B **89**, 235101 (2014).
[28] T. Iwasaki, F. Ishibashi, Y. Miyamoto, S. Kobayashi, T. Miyazaki, K. Tahara, K. D. Jahnke, L. J. Rogers, B. Naydenov, and F. Jelezko, Germanium-vacancy single color centers in diamond, Sci. Rep. **5**, 1 (2015).

[29] V. Ralchenko, V. Sedov, A. Khomich, V. Krivobok, S. Nikolaev, S. Savin, I. Vlasov, and V. Konov, Observation of the Ge-vacancy color center in microcrystalline diamond films, Bulletin of the Lebedev Physics Institute **42**, 165 (2015).

[30] E. A. Ekimov, S. G. e. Lyapin, K. N. Boldyrev, M. V. Kondrin, R. Khmelnitskiy, V. A. Gavva, T. y. V. Kotereva, and M. N. Popova, Germanium-vacancy color center in isotopically enriched diamonds synthesized at high pressures, JETP Lett. **102**, 701 (2015).

[31] K. Boldyrev, B. Mavrin, P. S. Sherin, and M. Popova, Bright luminescence of diamonds with Ge-V centers, J. Lumin. **193**, 119 (2018).

[32] M. Zaghrioui, V. N. Agafonov, and V. A. Davydov, Nitrogen and group-IV (Si, Ge) vacancy color centres in nano-diamonds: Photoluminescence study at high temperature (25 °C–600 °C), Mater. Res. Express **7**, 015043 (2020).

[33] N. A. Lozing, M. G. Gladush, I. Y. Eremchev, E. A. Ekimov, and A. V. Naumov, Stochastic superflares of photoluminescence from a single microdiamond with germanium-vacancy color centers: A general phenomenon or a unique observation, Phys. Rev. B **102**, 060301(R) (2020).

[34] T. Iwasaki, Y. Miyamoto, T. Taniguchi, P. Siyushev, M. H. Metsch, F. Jelezko, and M. Hatano, Tin-Vacancy Quantum Emitters in Diamond, Phys. Rev. Lett. **119**, 253601 (2017).

[35] E. Ekimov, S. Lyapin, and M. Kondrin, Tin-vacancy color centers in micro-and polycrystalline diamonds synthesized at high pressures, Diamond Relat. Mater. **87**, 223 (2018).

[36] S. D. Tchernij, T. Herzig, J. Forneris, J. Kupper, S. Pezzagna, P. Traina, E. Moreva, I. Degiovanni, G. Brida, and N. Skukan, Single-photon-emitting optical centers in diamond fabricated upon Sn implantation, ACS Photonics **4**, 2580 (2017).

[37] J. Goss, P. Briddon, M. Rayson, S. Sque, and R. Jones, Vacancy-impurity complexes and limitations for implantation doping of diamond, Phys. Rev. B **72**, 035214 (2005).

[38] S. Häußler, G. Thiering, A. Dietrich, N. Waasem, T. Teraji, J. Isoya, T. Iwasaki, M. Hatano, F. Jelezko, A. Gali, and A. Kubanek, Photoluminescence excitation spectroscopy of SiV^- and GeV^- color center in diamond, New J. Phys. **19**, 063036 (2017).

[39] Y. Chi, G. Chen, F. Jelezko, E. Wu, and H. Zeng, Enhanced photoluminescence of single-photon emitters in nanodiamonds on a gold film, IEEE Photonics Technol. Lett. **23**, 374 (2011).

[40] S. Kumar, V. A. Davydov, V. N. Agafonov, and S. I. Bozhevolnyi, Excitation of nanowire surface plasmons by silicon vacancy centers in nanodiamonds, Opt. Mater. Express **7**, 2586 (2017).

[41] S.-Y. Lee, M. Widmann, T. Rendler, M. W. Doherty, T. M. Babinec, S. Yang, M. Eyer, P. Siyushev, B. J. M. Hausmann, M. Loncar, Z. Bodrog, A. Gali, N. B. Manson, H. Fedder, and J. Wrachtrup, Readout and control of a single nuclear spin with a metastable electron spin ancilla, Nat. Nanotechnol. **8**, 487 (2013).

[42] R. John, J. Lehnert, M. Mensing, D. Spemann, S. Pezzagna, and J. Meijer, Bright optical centre in diamond with narrow, highly polarised and nearly phonon-free fluorescence at room temperature, New J. Phys. **19**, 053008 (2017).

[43] S. Lindner, A. Bommer, A. Muzha, A. Krueger, L. Gines, S. Mandal, O. Williams, E. Londero, A. Gali, and C. Becher, Strongly inhomogeneous distribution of spectral properties of silicon-vacancy color centers in nanodiamonds, New J. Phys. **20**, 115002 (2018).

[44] T. Lühmann, S. Diziain, J. Meijer, and S. Pezzagna, Identification and creation of the room-temperature coherently controllable ST1 spin center in diamond, ACS Photonics **9**, 1691 (2022).

[45] See Supplemental Material at http://link.aps.org/supplemental/10.1103/PhysRevB.107.L081406 for synthesis of diamonds, sample preparation, and descriptions of the experimental techniques and equipment; study of the annealing effect on diamonds; and spectral stability investigation.

[46] E. A. Ekimov, V. S. Krivobok, S. G. Lyapin, P. S. Sherin, V. A. Gavva, and M. V. Kondrin, Anharmonicity effects in impurity-vacancy centers in diamond revealed by isotopic shifts and optical measurements, Phys. Rev. B **95**, 094113 (2017).

[47] I. Y. Eremchev, A. Y. Neliubov, K. N. Boldyrev, V. G. Ralchenko, V. S. Sedov, L. Kador, and A. V. Naumov, Microscopic insight into the inhomogeneous broadening of zero-phonon lines of GeV–Color centers in chemical vapor deposition diamond films synthesized from gaseous germane, J. Phys. Chem. C **125**, 17774 (2021).

[48] N. L. Naumova, I. A. Vasil'eva, A. V. Naumov, and I. S. Osad'ko, Evaluation of parameters of intramolecular interaction from absorption and fluorescence spectra of substituted arylpolyene with poor resolved vibrational structure, J. Lumin. **111**, 37 (2005).

[49] S. Zhu, Q. Meng, L. Wang, J. Zhang, Y. Song, H. Jin, K. Zhang, H. Sun, H. Wang, and B. Yang, Highly photoluminescent carbon dots for multicolor patterning, sensors, and bioimaging, Angew. Chem. Int. Ed. **52**, 3953 (2013).

[50] S. Choi, V. N. Agafonov, V. A. Davydov, L. F. Kulikova, and T. Plakhotnik, Formation of interstitial silicon defects in Si- and Si,P-doped nanodiamonds and thermal susceptibilities of SiV− photoluminescence band, Nanotechnology **31**, 205709 (2020).

[51] E. Togan, Y. Chu, A. S. Trifonov, L. Jiang, J. Maze, L. Childress, M. V. G. Dutt, A. S. Sørensen, P. R. Hemmer, A. S. Zibrov, and M. D. Lukin, Quantum entanglement between an optical photon and a solid-state spin qubit, Nature (London) **466**, 730 (2010).

[52] M. K. Bhaskar, D. D. Sukachev, A. Sipahigil, R. E. Evans, M. J. Burek, C. T. Nguyen, L. J. Rogers, P. Siyushev, M. H. Metsch, H. Park, F. Jelezko, M. Lončar, and M. D. Lukin, Quantum Nonlinear Optics with a Germanium-Vacancy Color Center in a Nanoscale Diamond Waveguide, Phys. Rev. Lett. **118**, 223603 (2017).

[53] A. Beveratos, R. Brouri, T. Gacoin, A. Villing, J.-P. Poizat, and P. Grangier, Single Photon Quantum Cryptography, Phys. Rev. Lett. **89**, 187901 (2002).